ORIGINAL ARTICLES

Observations of Extreme Waves and Wave Spectra during Hurricane Dorian (2019)

Brandon J. Bethel 0000-0001-5312-091X
University of The Bahamas

Abstract

Due to the sparse distribution of buoys in the ocean, direct observations of extreme wave activity as excited by tropical cyclones (TCs) are few; but nonetheless, these buoys provide rare opportunities to learn more about how weather systems interact with the ocean wave field. In this study, National Oceanic and Atmospheric Administration National Data Buoy Center buoy observations of one-dimensional (1D) and two-dimensional (2D) wave spectra during the translation speed of Hurricane Dorian (2019) through the Atlantic Ocean were used to examine extreme wave events in the days before and after its September 1, 2019 landfall in The Bahamas. Observations of wave properties during storm intensification and decay showed that although significant wave height naturally rose and fell, the dominant wave period remained virtually constant. At the height of the storm, a lethal combination formed, with the highest significant wave heights being recorded at over 8 m (more than four times the mean) and dominant wave periods exceeded 12 s. Wave direction also varied widely as wave regimes shifted from wind-sea to swell, with spectral wave energy peaking at over 120 m^2/Hz, six times higher than pre-Hurricane Dorian wave states. This study provides the first in situ characterization of extreme wave heights as induced by Hurricane Dorian. The study recommends that a number of observational platforms be funded, developed, and deployed throughout the Lucayan Archipelago.

DOI: 10.15362/ijbs.v29i1.497

Introduction

On ancient and modern battlefields alike, scouts play an important role. Along with the information they acquire, or fail to acquire, scouts can serve as the deciding factors of a war's outcome. In a similar way, for the oceanographic community, instruments placed in the coastal and open ocean act as scouts, providing invaluable observations that satisfy not only humanity's scientific curiosity, but also serve coastal communities directly through supporting a plethora of ocean engineering, maritime, and renewable energy activities, or indirectly by validating reanalysis or numerical model output (Garcia et al., 2018; Ardhuin et al., 2019; De May-Frémaux et al., 2019). Under force by tropical cyclones (TCs), the ocean deviates strongly from its mean state. As is abundantly clear for small island developing states (SIDS), most recently seen by the September 1, 2019 landfall of Hurricane Dorian in The Bahamas, extreme wave states and storm surge can cause immense and incalculable loss of life and property (Greig et al., 2020).

Consequently, observations of wave states excited by TCs can deepen theoretical understanding and improve forecasting abilities so that coastal defense schemes and mitigation approaches can be augmented and optimized to minimize catastrophic damage (Liu et al., 2021) and make maritime activities safer (Bell & Kirtman, 2019; Campos et al., 2020; Støle-Hentschel et al., 2020; Chen et al., 2021). These improvements are especially important in the context of increasing TC intensity, shifting atmospheric patterns, and more prevalent extreme wave climates (Shimura et al., 2016; Timmermans et al., 2018; Markina et al., 2019).

Scientists use a diverse array of tools to observe ocean wave state under TC forcing. These tools run the gamut from in situ instruments to remote sensing to numerical simulations. For example, Ranji et al. (2020) studied Cyclone Ashobaa-induced waves and their spectra in the Gulf of Oman using Acoustic Doppler Current Profilers (ADCPs) and Acoustic Wave and Current (AWAC) profiler subsurface buoys. They found that when the cyclone was far away from measuring stations, wave spectra were observed to be bimodal or trimodal, with this shifting to unimodal spectra when cyclones were near to measuring stations. At landfall, wave spectra once again became bimodal due to the simultaneous influence of local wind-seas and swell. Further, Hwang and Walsh (2018) used remotely sensed observations of hurricane-directional wave spectra to establish a model describing dominant wave propagation directions. Although the model was successful in nine of the 11 datasets available for investigation, a hurricane's proximity to a coast (i.e., landfalling) and rapid changes in translation speed/direction were responsible for significantly differing statistics of the remaining two datasets. Within the Caribbean Sea and the adjacent Atlantic Ocean, Ortiz-Royero et al. (2013) used a virtual buoy extracted from WaveWatch III reanalysis to study extreme wave events induced by cold fronts. They found that, in addition to storms and hurricanes, cold fronts should also be considered when evaluating average and extreme wave regimes. Otero et al. (2016) identified that while both storms and cold fronts can cause extreme wave regimes in the Colombian Caribbean coastal region, extreme wave heights caused by TCs have different effects than cold fronts along the Colombian coast. In the South Atlantic, Gramcianinov et al. (2021) showed that extreme waves could occur both behind and ahead of a cyclone's cold front, in addition to along its warm front. The study additionally identified that the anticyclone position relative to a given cyclone could play a crucial role in extreme wave formation through the increase of the horizontal pressure gradient and thus surface wind speed. This could affect a TC's translation speed, which determines the position of the fetch and associated wave generation processes. This concept received confirmation in a study of sea breeze and TC wave spectra evolution conducted by Nair et al. (2021) in another basin (the Bay of Bengal). Nair et al.'s numerical study showed that TC-generated waves are mostly young wind-seas which do not exactly follow the wind field but are dependent on the TC's forward motion velocity. Ponce de León and Bettencourt (2019) demonstrated through satellite altimetry observations and composite analysis of North Atlantic extra-tropical cyclone waves that due to the extended fetch mechanism, higher waves can be found in the south-eastern quadrant of a cyclone, and the highest waves are found during the 48-hour period when the TC's strength is at its maximum.

Crucial for this study, although Montoya et al. (2018) estimated an increase in the occurrence of extreme wave heights in the

eastern and central Caribbean, few studies of extreme wave heights in the Atlantic Ocean east of the Lucayan Archipelago (consisting of sovereign Bahamas and U.K.-dependent Turks and Caicos Islands) exist. However, Bell and Kirtman (2019) and Sahoo et al. (2019) both identified the vulnerability of the archipelago and ships to extreme waves. Consequently, due to dual regional limitations in technological capability and availability (i.e., there are no known coastal high-frequency radars dedicated to oceanographic applications), this study employs National Data Buoy Center (NDBC) buoy and merged satellite altimeter observations of extreme wave states and spectra as excited by Hurricane Dorian (2019) during its slow translation speed through the adjacent Atlantic Ocean before and after its landfall in The Bahamas. This is justified as Collins et al. (2018) demonstrated the efficacy of buoys in observing wave spectra even under the TC influence.

Datasets and Methodology

Satellite Altimeter Dataset

To study the mean significant wave height (the average of the highest one-third of all waves measured over a particular period) state for a baseline to which the extreme wave states induced by Hurricane Dorian (2019) can be compared, the gridded L4 near-real time (NRT) multi-mission (Jason-3, Sentinel-3A, SARAL/Altika) wind/wave product was acquired from AVISO (https://www.aviso.altimetry.fr/). The dataset is available on a spatial resolution of 1° × 1° within the 60°W–80°W and 20°N–30°N geographical space, and at a daily temporal resolution ranging from September 2009 to December 2019.

In Situ Dataset

Three buoys deployed in the Atlantic Ocean east of the Lucayan Archipelago (Figure 1, Table 1) were examined. These buoys are owned and operated by the NDBC (https://www.ndbc.noaa.gov/) and captured extreme wave states. NDBC buoys have been extensively validated to produce robust observations of wave and wind properties, justifying their usage in this study, as in others (e.g., Tamizi & Young, 2020; Ribal & Young, 2020; Wang et al., 2020; Pramudya et al., 2021). Observations of one-dimensional (1D) frequency spectra and two-dimensional (2D) directional functions were used to estimate significant wave height, dominant wave period, and dominant wave direction.

This study focuses on Hurricane Dorian (2019), a Category 5 hurricane that had a minimum central pressure of 910 hPa and wind speeds exceeding ~295 km/h (~82 m/s). Hurricane Dorian made landfall in the northern Bahamas on September 1, 2019. Data concerning the hurricane were acquired from the National Hurricane Center (https://www.nhc.noaa.gov/). The storm was notable in that it was the strongest hurricane on record to make landfall in The Bahamas and possessed a remarkably slow translation speed (~1.4−2 m/s), which may have contributed to extreme wave and storm surge development.

Figure 1 *Geographic Map of the Lucayan Archipelago with the Best-track of Hurricane Dorian in the Study Area and National Data Buoy Center (NDBC) Buoy Locations*

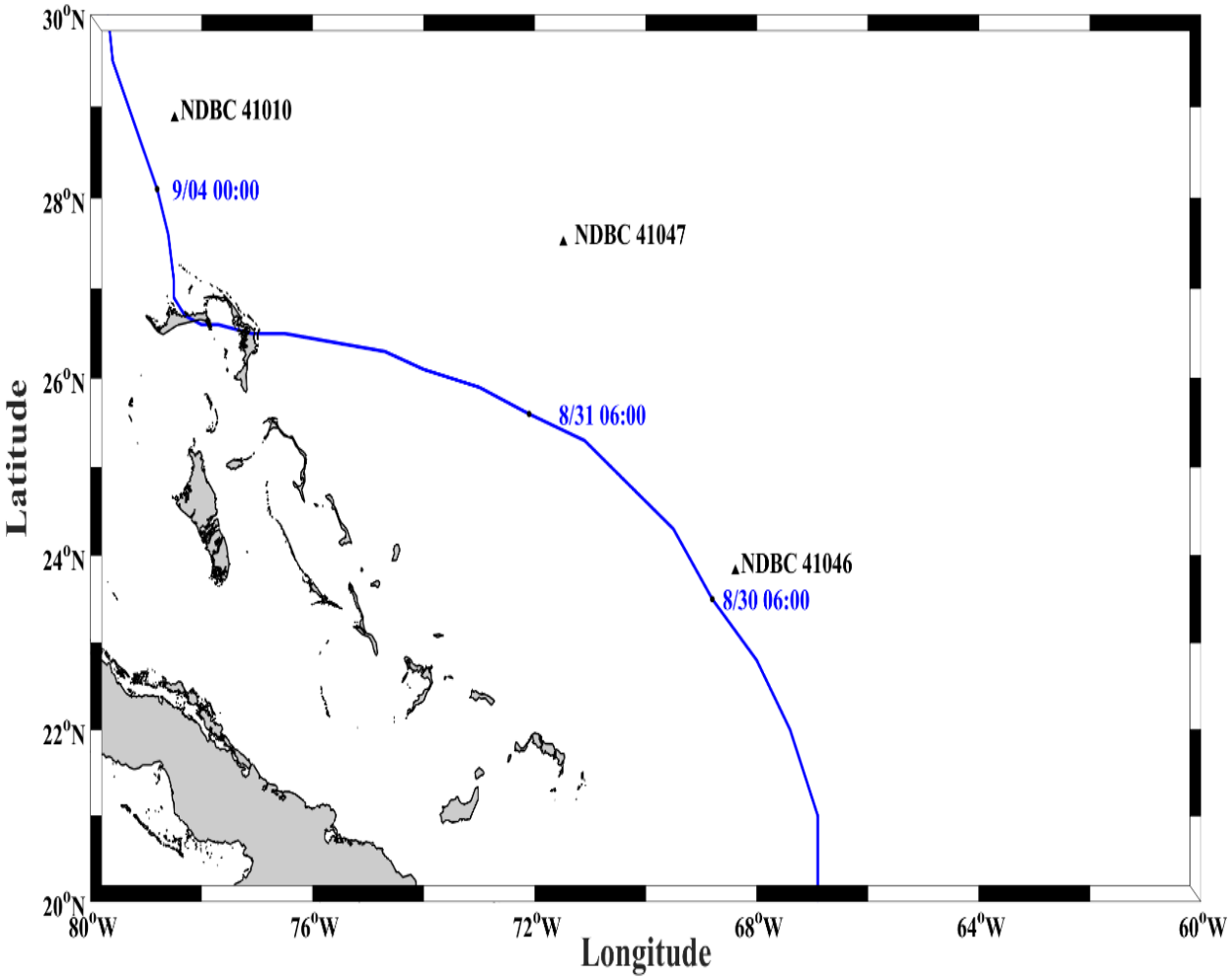

Table 1 *National Data Buoy Center (NDBC) Buoy Statistics*

NDBC ID	Latitude (°N)	Longitude (°W)	Water Depth (m)
41010	28.878	78.485	890
41046	23.822	68.384	5549
41047	27.514	71.494	5321

Methodology

Wave Spectra

As described by Hanson and Jensen (2004), and Hanson et al. (2009), wave spectra from NDBC buoys are computed at an hourly resolution from 20-min records over a frequency band of 0.03–0.4 Hz. Reported quantities include the nondirectional (1D) energy-frequency spectrum $E(f)$, for directional buoys, the vector mean direction $\bar{\theta}f$, and the directional distributional parameters. These can be described by the Longuet-Higgins Fourier coefficients a_1, a_2, b_2, and b_2 as:

$$r_1 = \frac{\sqrt{a_1^2+b_1^2}}{a_\circ} \quad (1)$$

$$r_2 = \frac{\sqrt{a_2^2+b_2^2}}{a_\circ} \quad (2)$$

$$\alpha_1 = 270 - tan^{-1}(b_1/a_1) \quad (3)$$

$$\alpha_2 = 270 - \frac{tan^{-1}(b_1/a_1)}{2} + \{0,180\} \quad (4)$$

where $a_\circ = E(f)$. NDBC reports wave measurement accuracies are $\pm$0.2 m in wave height, $\pm$1.0 s in wave period, and $\pm$10° in wave direction. Following Zhang et al. (2015), in turn citing Longuet-Higgins et al. (1963), wave directional spectra using the directional Fourier series expansion can be estimated as:

$$a_0 = \frac{C_{11}}{\pi} \quad (5)$$

$$a_1 = \frac{Q_{12}}{k\pi} \quad (6)$$

$$b_1 = \frac{Q_{13}}{k\pi} \quad (7)$$

$$a_2 = \frac{C_{22}-C_{33}}{k^2\pi} \quad (8)$$

$$b_2 = \frac{2C_{23}}{k^2\pi} \quad (9)$$

where

$$Q_{12} = kC_{11}r_1\cos(\theta_1) \quad (10)$$

$$Q_{13} = kC_{11}r_1\sin(\theta_1) \quad (11)$$

$$C_{23} = \frac{1}{2}k^2C_{11}r_1\sin(2\theta_2) \quad (12)$$

$$C_{22} - C_{33} = k^2C_{11}r_2\cos(2\theta_2) \quad (13)$$

where $C_{11}, C_{22}, Q_{12}, Q_{13}, a_0, a_0, a_1, a_2, b_1,$ and b_2 are all frequency functions f, and k is the wavenumber. The directional frequency spectrum is given as:

$$S(f,\theta) = \frac{a_0}{2} + a_1\cos(\theta) + b_1\sin(\theta) + b_1\cos(\theta) + b_2\sin(\theta) \quad (14)$$

Adding weighting values to prevent negative energy, the directional frequency spectrum is given by:

$$S(f,\theta) = \frac{a_0}{2} + \frac{2}{3}[a_1\cos(\theta) + b_1\sin(\theta)] + \frac{1}{6}[a_2\cos(\theta) + b_2\sin(\theta)] \quad (15)$$

Following this, the directional frequency spectra $S(f,\theta)$ can be transformed into the 2D wave spectra $S(f,\theta)$ in the following two steps. Firstly, the intermediate expression $S(k,\theta)$ should be expressed in terms of the frequency $S(f,\theta)$ by the Jacobian:

$$S(k,\theta) = S(f,\theta)\frac{df}{dk} = \frac{S(f,\theta)g}{8\pi^2 f}[\tanh(kh) + \frac{kh}{cosh^2(kh)}] \quad (16)$$

Then, $S(k,\theta)$ is expressed with respect to $S(k_x,k_y)$ as:

$$S(k_x,k_y) = S(k,\theta)\frac{\partial(k,\theta)}{\partial(k_x,k_y)} = \frac{S(k,\theta)}{k} \quad (17)$$

where h is the water depth and g is the gravitational acceleration. Using this method,

all three parameters which can describe the wave system (i.e., the significant wave height, the dominant wave period, and wavelengths) can be acquired. However, this study focuses only on the former two in addition to dominant wave direction. The significant wave height, as an example, can be extracted from the above through the square root of the energy spectrum's variance multiplied by four.

Results

Mean Wave States

Before examining extreme wave states during the passage of Hurricane Dorian through the Atlantic Ocean, I consider mean significant wave height states over the 10-year period of September 2009–December 2019. As shown in Figure 2, deep in the Atlantic Ocean, the mean significant wave height could reach a maximum of 2 m. This gradually decreases towards the east over the Lucayan Archipelago at ~1.2 m to a minimum of ~1 m east of The Bahamas and in Cuban coastal waters. These wave heights are forced by the prevailing trade winds, but the moderate gradation over the Lucayan Archipelago is caused by island sheltering effects. These results are confirmed by in situ observations. Table 2 shows average significant wave height for each NDBC buoy over the 10-year period, the average mean and dominant wave periods, and wave direction. This sector of the Atlantic Ocean has a very mild wave climate (Guillou et al., 2020) but, as will be shown in subsequent sections, wave properties are pushed towards the extreme under hurricane forces.

Figure 2 *Mean Significant Wave Height (m) September 2009-December 2019*

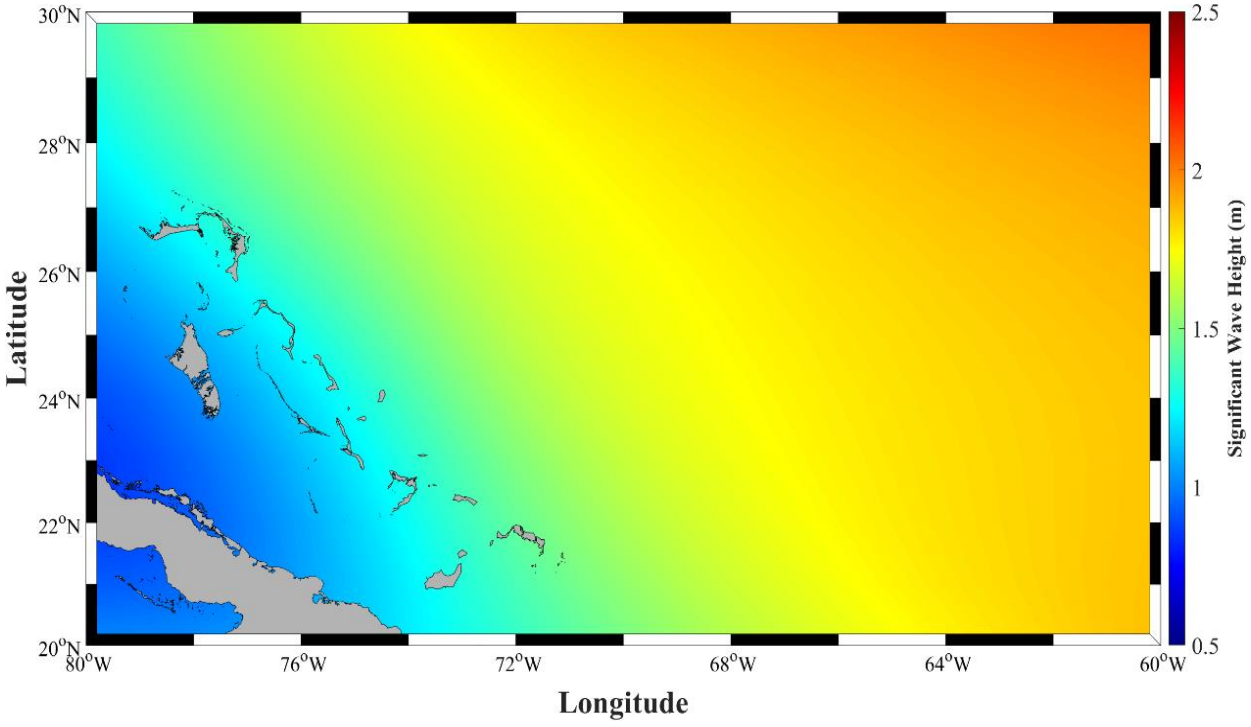

Note: As derived from the Merged Satellite Altimeter product east of the Lucayan Archipelago.

Table 2 *Mean Wave Properties January 2009–December 2019*

NDBC ID	Significant Wave Height (m)	Mean Wave Period (s)	Dominant Wave Period (s)	Mean Wave Direction (°)
41010	1.50	5.45	8.11	116.73
41046	1.72	5.98	8.89	103.22
41047	1.68	6.12	8.83	119.29

Note: As observed by the in situ buoy platforms. Additional months were added due to the large gaps that exist in each buoy dataset

Extreme Wave Spectra

This section describes wave frequency (1D) and directional (2D) spectra, as observed during the growth, peak, and decay of Hurricane Dorian as the system passed by each buoy. Figure 3 presents observations of 1D wave frequency spectra as recorded by NDBC buoy 41046 from August 30 UTC 0200. Due to the geographical location of this buoy, the front-right quadrant of Hurricane Dorian faced the buoy, allowing wind waves propagating out to increase the wave spectral density from 30 m^2/Hz at 0200 UTC August 30 (Figure 2a) to over 80 m^2/Hz two hours later (Figure 2b). From 0200–0600 UTC, the frequency spectra were single-peaked, before forming a second peak at 0600 (Figure 2c) and becoming bimodal, indicating the influence of swell. In Figures 3d-f, the bimodal spectrum was maintained from 0800 to 1200, respectively, though in Figure 3e, the two peaks are much different in size. At UTC 1200, spectral density returned to its pre-Hurricane Dorian levels but remained bimodal, continuing the dominance of swell. Thus, in Figure 4 where the corresponding 2D wave spectra are shown, it can be observed that waves propagated towards the northeast, congruent with the translation direction of Hurricane Dorian. Further, spectral density fluctuates with the storm's growth and decay. Interestingly, when the 1D wave spectra frequency in Figures 3d and 3f are bimodal, the corresponding 2D wave spectra during the times of wind-sea (UTC 0200–0600, 1000) are well defined, but they become distorted when more than one peak appears, signalling the disturbance of wind-sea with swell.

Figure 3 *Observations of 1D Wave Frequency Spectra for NDBC Buoy 41046 during Hurricane Dorian on August 30*

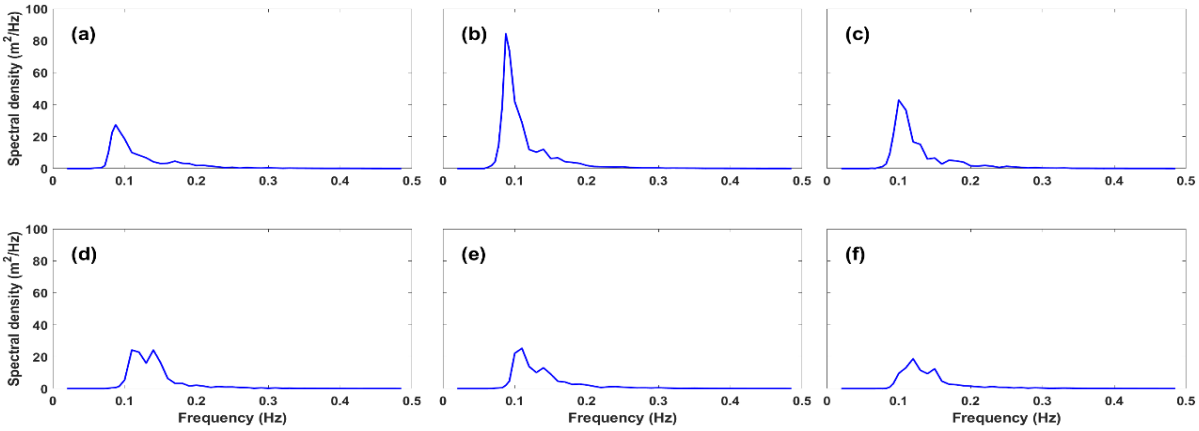

Note: UTC (a) 0200, (b) 0400, (c) 0600, (d) 0800, I 1000, and (f) 1200

Figure 4 *Same as Figure 3, But for Observations of 2D Wave Spectra*

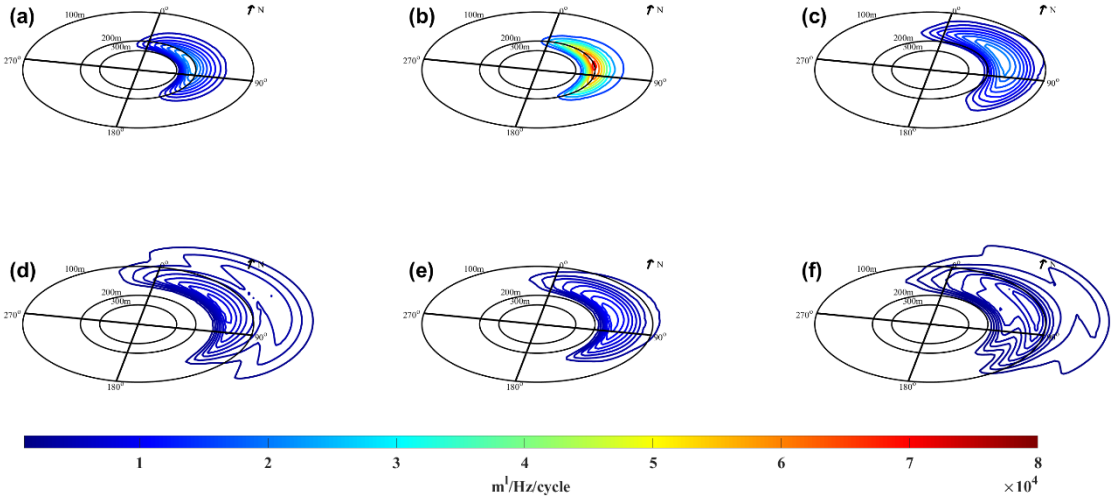

Further along Hurricane Dorian's translation through the Atlantic Ocean on its way to The Bahamas, Figure 5 contains 1D wave frequency spectra as recorded by NDBC buoy 41047 from August 30 to August 31. Here, due to this buoy's distance from the storm (Figure 1), extreme wave states generated by Hurricane Dorian could not be observed in the fine detail seen in the previous discussion. Nonetheless, growth 1D wave frequency spectra can be observed as the storm approached (Figure 5a-c). From August 30 UTC 2300 to August 31 UTC 0400, the 1D wave spectra stayed under 20 m^2/Hz, but its shape was abnormally multimodal. Over the following four hours (UTC 0600, 0800, Figures 5d and 5e, respectively), more traditional spectra appeared and remained largely unimodal until UTC 1000 where a well-defined second peak appeared. At no time did the spectral density approach 25 m^2/Hz, reflecting the great distance between the system and NDBC buoy 41047.

Figure 5 *Observations of 1D Wave Frequency Spectra for NDBC Buoy 41047 during Hurricane Dorian*

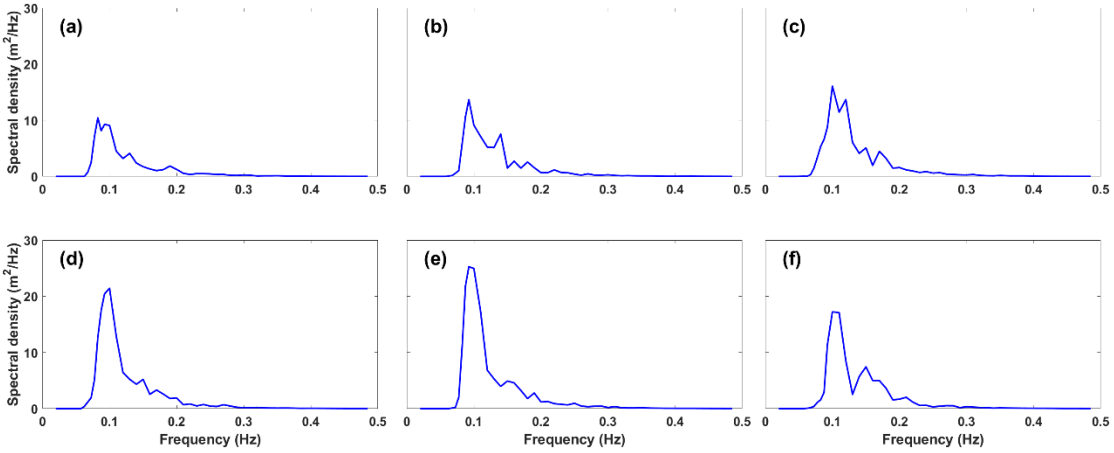

Note: (a) August 30 UTC 2300 followed by August 31 UTC (b) 0200, (c) 0400, (d) 0600, (e) 0800, and (f) 1000

Corresponding observations of 2D wave spectra for Figure 6 are presented in Figure 5. Similar to the previous case, wave spectral energy increased as the storm intensified from August 30 UTC 2300 to August 31 UTC 0400 but, at this stage, waves propagated away from the system, towards the southeast. Interestingly, only minor distortion can be observed in the 2D wave spectra in Figures 6b, 6c, and 6f during bimodal or multimodal 1D spectra shown in Figures 5b, 5c, and 5f.

Figure 6 *Same as Figure 5, But For Observations of 2D Wave Spectra*

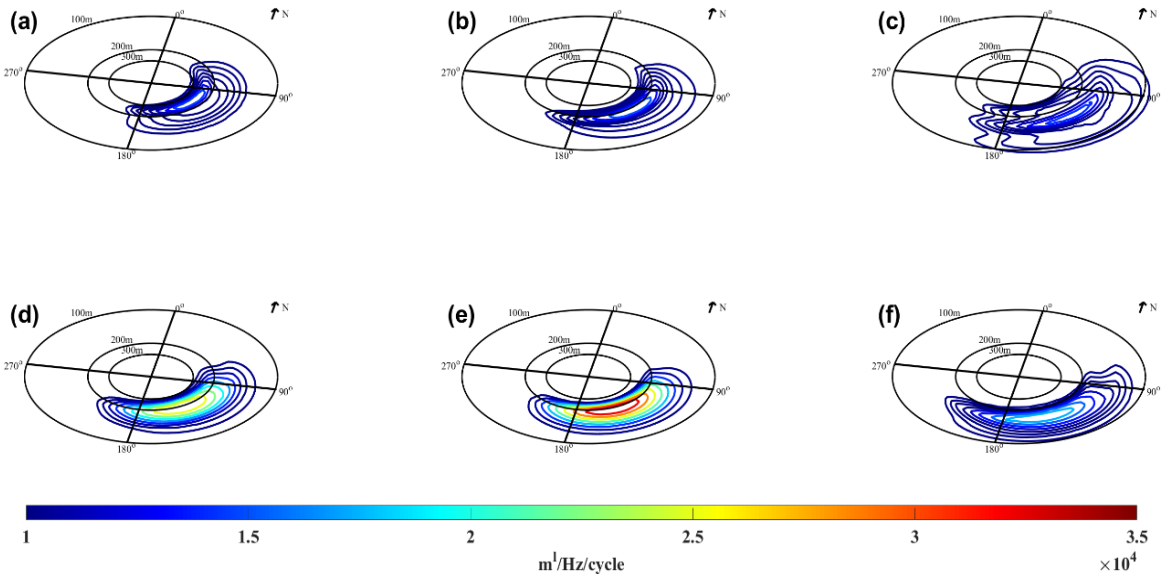

Although no platforms were available to observe extreme wave heights in The Bahamas during the September 1, 2019 landfall of Hurricane Dorian, NDBC buoy 41010 captured extreme wave activities three days later following a brief period of intermittency. Figure 7a shows that wave spectral density exceeded 100 m^2/Hz on September 4 UTC 1000, before increasing to nearly 120 m^2/Hz two hours later (Figure 7b). As shown in Figures 8c-f, as the hurricane continued its slow, northward translation, spectral density decreased gradually to return to below 50 m^2/Hz, though this value is still much higher than pre-Hurricane Dorian levels. Although 1D spectra for the most part are single-peaked, indicating the dominance of wind waves, minor deviations from this can be observed with a secondary peak appearing most noticeably in Figures 7a, 7b, and 7d.

Figure 7 *Observations of 1D Wave Frequency Spectra for NDBC Buoy 41010 during Hurricane Dorian on September 4*

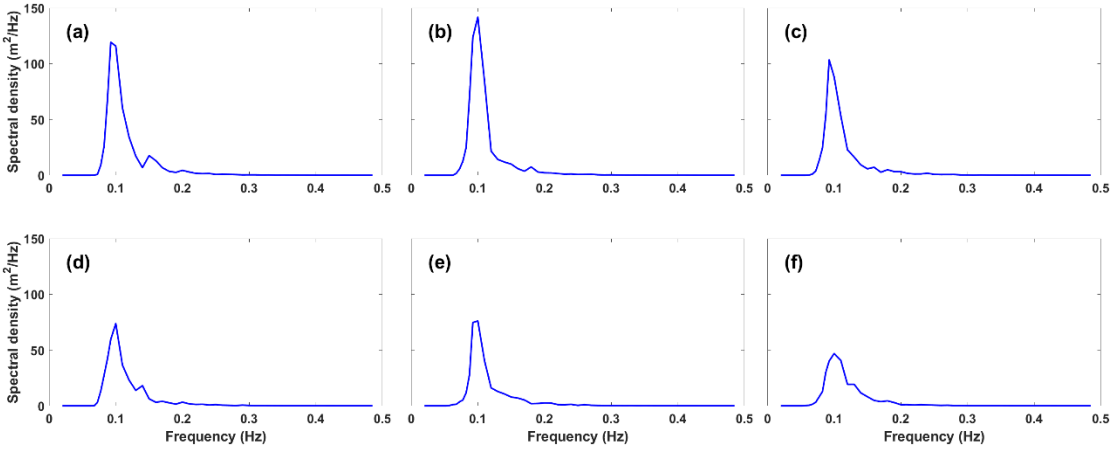

Note: UTC (a) 1000, (b) 1200, (c) 1400, (d) 1600, (e) 1800, and (f) 2000

Figure 8 gives the 2D wave spectra which accompany the 1D spectra of Figure 6. Here, spectral density can be observed to grow as the storm grew more intense, with the directional wave spectra maintaining a high degree of coherency, indicating a single wave regime. Waves continued to propagate towards the north-east, again congruent with the forward right-hand quadrant of Hurricane Dorian and its translation direction.

Figure 8 *Same as Figure 7, But For Observations of 2D Wave Spectra*

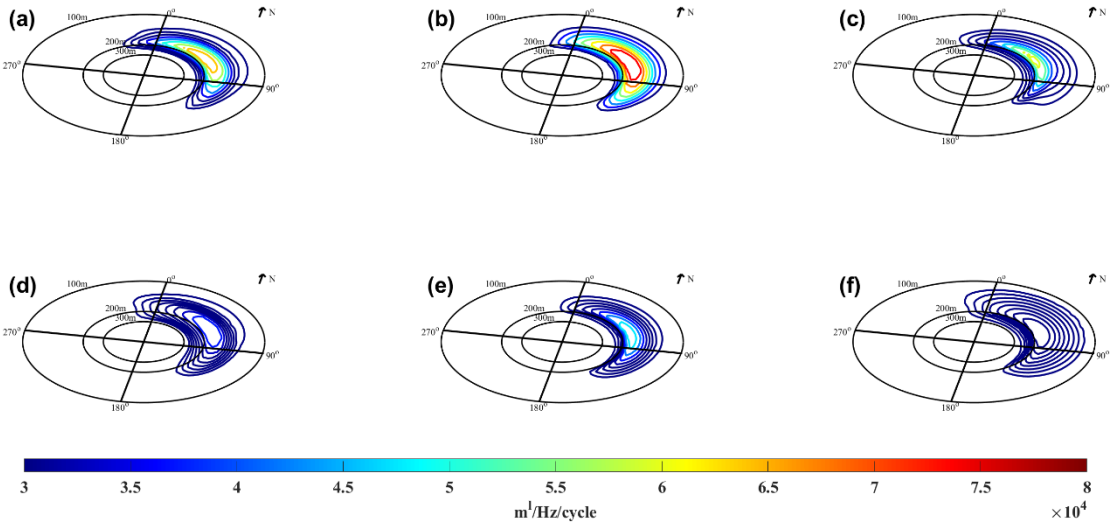

Extreme Wave States

Following the examination of extreme 1D and 2D wave spectra, wave properties as computed by observations of wave spectral frequency and directional functions for each NDBC are presented in Tables 2–4. In Table 3 wave properties of Hurricane Dorian were calculated by NDBC 41046 from August 30 UTC 0200–1200, it can be observed that as the storm increased in intensity, wave heights increased from 4.2 m on UTC 0200 to a maximum of 6.2 m two hours later, before steadily decreasing to 3.8 m. The dominant wave period, by contrast, steadily decreased over time from 11.4 s to 8.3 s but remained well above normal conditions, with low-period, highly energetic swell characterizing the wave field before transitioning back to the mean state. Dominant wave directions also fluctuated throughout the growth and decay of the storm. During system intensification, the wave direction reduced minutely from the 103.22° mean before shifting a colossal +76° after the wave heights decreased to 4.5 m at UTC 0800. Two hours later at UTC 1000, wave directions again fell below the mean and continued to decrease over two hours to the 86.3° minimum.

Table 4 measures extreme wave states for the following day for NDBC buoy 41047, which lay far from the storm's direct influence. Yet, the buoy still registered significant wave heights at twice the western Atlantic Ocean average value of 1–2.5 m. It achieved a maximum of 4.1 m on August 31 UTC 0800 with a corresponding dominant wave period of 11.3 s. At this point, and with reference to Table 2, significant wave heights were over twice the mean value (1.68 m) and the dominant wave period lengthened over 2 s, generating a highly energetic sea state. Over the course of the storm, as it transitioned pass NDBC buoy 41047, the dominant wave direction also fluctuated widely. This direction deviated from the local mean of 119.29 by up to +60° following the peak of the storm on August 31 UTC 1000.

Table 3 *Wave Properties Calculated from Observations of 1D Frequency and Directional Functions by NDBC Buoy 41046 over August 30 UTC 0200–1200*

UTC	Significant Wave Height (m)	Dominant Wave Period (s)	Dominant Wave Direction (°)
0200	4.2	11.4	92.3
0400	6.2	11.4	96.8
0600	5.0	10.0	88.3
0800	4.5	9.1	179.0
1000	4.2	10.0	91.7
1200	3.8	8.3	86.3

Table 4 *Wave Properties Calculated from Observations of 1D Frequency and Directional Functions by NDBC Buoy 41047 over August 30 UTC 2300 and August 31 UTC 0200–1000*

UTC	Significant Wave Height (m)	Dominant Wave Period (s)	Dominant Wave Direction (°)
2300	2.8	12.2	149.9
0200	3.1	10.8	152.5
0400	3.6	10.0	152.7
0600	3.9	11.2	164.4
0800	4.1	11.3	168.7
1000	3.6	10.0	178.3

Table 5 presents the most extreme wave properties calculated from observations of 1D frequency and directional functions by NDBC buoy 41010 from September 4 UTC 1000 – 2000. There, the minimum significant wave height was estimated at 5.7 m, which is nearly four times the mean previously observed in Table 2. The maximum wave height (8.2 m), naturally, was even more extreme and represented heights over five times higher than normal conditions. Similarly, the dominant wave period lengthened from the mean 8.11 s to over 10 s. Although the maximum of 10.8 s measured at UTC 1400 was not the most extreme (see Table 4, UTC 2300 where the significant wave height and wave period were measured at 2.8 m and 12.2 s, respectively), its combination with large 7.1 m waves ensured that, at this moment, an even more extreme wave state was achieved. The dominant wave direction shifted from the mean of 116.73° to a minimum of 71.6° and a maximum of 88°.

Table 5 *Wave Properties Calculated from Observations of 1D Frequency and Directional Functions by NDBC Buoy 41010 from September 4 UTC 1000–2000*

UTC	Significant Wave Height (m)	Dominant Wave Period (s)	Dominant Wave Direction (°)
1000	7.9	10.7	71.6
1200	8.2	10.6	84.1
1400	7.1	10.8	75.5
1600	6.4	10.6	84.1
1800	6.2	10.6	88.01
2000	5.7	10.6	75.5

Discussion

Due to the mild wave climate enjoyed by small island developing states (SIDS) of the Caribbean Sea, researchers investigating extreme waves in more hostile wave environments (e.g., Yang & Oh, 2018; Babanin et al., 2019; Derkani et al., 2021) may not find the results of this paper particularly worrying. The large ocean-to-land ratios and extreme vulnerability to climate change of SIDS (Scandurra et al., 2018; Thomas et al., 2020), and, in particular The Bahamas' special sensitivity to extreme waves and storm surge (Sahoo et al., 2019), intense research in this field is required. Support for the present results of wave period lengthening and wave height growth is found in observations performed by Tian et al. (2020) who studied three South China Sea TCs. However, due to SIDS' limited financial strength and technological capabilities, observation platforms are very limited. Hurricane Dorian did not excite the record observed extreme heights of 16.91 m as induced by Hurricane Katrina (2005) in the Gulf of Mexico (Bouchard et al., 2006), but the 8 m wave heights observed in this study are roughly equivalent to the wave heights that sunk the El Faro by Hurricane Joaquin-induced extreme waves in 2015 (Fedele et al., 2017). They are also directly responsible for catastrophic loss of life and property in the northern Bahamian islands of Abaco and Grand Bahama (Zegarra et al., 2020).

However, buoys and other observational platforms (e.g., high-frequency coastal radars) are expensive and their development and installation are not a current priority of the Bahamas government. The absence of wave measurements in the nearshore represents a major blind spot, especially considering the archipelago's vulnerability to hurricane-induced extreme waves and storm surge. The lack of measuring tools minimizes opportunities to learn from Hurricane Dorian and other extreme events. It also weakens countries' abilities to predict, prepare for and respond to future extreme weather events. The present lack of instruments, weather buoys, or high frequency coastal radar can be temporarily dealt with by using numerical models, reanalysis, or satellite sources of data (e.g., Takbash & Young, 2019; Meucci et al., 2020), but these are no substitute for physical instruments. Considering the strong likelihood of more frequent and volatile hurricanes, ocean observational blind spots should be eliminated as soon as possible. This investment could be financed through a $200 million Inter-American Development Bank loan recently made available to The Bahamas to minimize loss in life and economic productivity.

Conclusion

Extreme waves and ocean states induced by TC activity threaten and can potentially upend SIDS and coastal communities. As such, observing these events is acutely important. Using a merged satellite altimeter significant wave height product as a baseline, this study accessed three NDBC buoys off the coast of the Lucayan Archipelago to study extreme waves and spectra induced by Hurricane Dorian. In this study, calculations suggested that the highest waves could range anywhere from 3–8 m, with the dominant wave period lengthening from 8 s to over 12 s, forming a lethal wave state. Observations of 1D spectra indicated that wind waves dominated the wave field as expected. This is due to direct energy input from hurricane winds into wave generation. However, observations also show that swell contributed to the total wave field and shifted previously single-peaked wave spectra into double-peaked, bimodal spectra in many cases, and into multimodal spectra in a few others. Spectral energy densities ranged from 30 m^2/Hz just before the arrival of the storm at NDBC buoy 41047 to over 80 m^2/Hz during

the storm, before gradually decreasing to pre-Hurricane Dorian levels. A similar pattern of growth and decay was observed at NDBC buoy 41047 but, due to the storm's distance from the buoy, energy densities remained under 30 m^2/Hz. At NDBC buoy 41010, however, spectral wave density was observed at approximately 120 m^2/Hz on September 4 UTC 1200, three days after Hurricane Dorian made landfall in The Bahamas. Over the course of the following eight hours, it decayed to just under 50 m^2/Hz, which is still over twice that of pre-Hurricane Dorian states, highlighting the drastic departure from mean to extreme ocean states.

This study was limited by the quantity and quality of observational data that could have captured extreme wave states in even finer detail at the point of landfall in The Bahamas. Although alternative tools such as numerical models or reanalysis datasets could be employed in future studies, strategies to circumvent the current technological gaps should be devised and readily applied as The Bahamas and other SIDS attempt to evolve into large ocean states which are more than just climate resilient.

Acknowledgments: This study thanks the National Data Buoy Center for providing the datasets.

Funding: No funding was received to conduct this study.

Conflicts of Interest: The authors declare no conflicts of interest.

References

Ardhuin, F., Stopa, J. E., Chapron, B., Collard, F., Husson, R., Jensen, R. E., Johannessen, J., Mouche, A., Passaro, M., Quartly, G. D., Swail, V., & Young, I. (2019). Observing sea states. *Frontiers of Marine Science, 6,* 124. https://doi.org/10.3389/fmars.2019.00124

Babanin, A.V., Rogers, W. E., de Camargo, R., Doble, M., Durrant, T., Filchuk, K., Ewans, K., Hemer, M. Janssen, T., Kelly-Gerreyn, B., Machutchon, K., McComb, P., Qiao, F., Schulz, E., Skvortsov, A., Thomson, J., Vichi, M., Violante-Carvalho, N., Wang, D. … Young, I. R. (2019). Waves and swells in high wind and extreme fetches, measurements in the Southern Ocean. *Frontiers in Marine Science, 6,* 361. https://doi.org/10.3389/fmars.2019.00361

Bell, R., & Kirtman, B. (2019). Extreme environmental forcing on the container ship SS El Faro. *Journal of Operational Oceanography, 14*(2), 98–113. https://doi.org/10.1080/1755876X.2019.1684136

Bouchard, R. H., Teng, C. C., & Hervey, R. V. (2006). Significant events reported by the NDBC stations during Hurricane Katrina. *IEEE, OCEANS 2006.* https://doi.org/10.1109/OCEANS.2006.306817

Campos, R.M., D'Agostini, A., Leite França, B. R., Machado Cruz, L., & Guedes Soares, C. (2020). Extreme wind and wave predictability from operational forecasts at the Drake Passage. *Journal of Offshore Mechanics and Arctic Engineering, 143*(2), 1–16. https://doi.org/10.1115/1.4048151

Chen, C., Sasa, K., Prpić-Oršić, J., & Mizojiri, T. (2021). Statistical analysis of waves' effects on ship navigation using high-resolution numerical wave simulation and shipboard measurements. *Ocean Engineering, 229*(10), 108757. https://doi.org/10.1016/j.oceaneng.2021.108757

Collins, C.O., Potter, H., Lund, B., Tamura, H., & Graber, C. (2018). Directional wave spectra observed during intense tropical cyclones. *Journal of Geophysical Research: Oceans, 123*(2), 773–793. https://doi.org/10.1002/2017JC012943

De May-Frémaux, P., Ayoub, N., Barth, A., Brewin, R., Charria, G., Campuzano, F., Ciavatta, S., Cirano, M., Edwards, C. A., Federico, I., Gao, S., Garcia Hermosa, I., Garcia Sotillo, M., Hewitt, H., Hole, L. R., Holt, J., King, R., Kourafalou, V., Youyu, L. … Xueming, Z. (2019). Model-observations synergy in the coastal ocean. *Frontiers in Marine Science, 6*, 436. https://doi.org/10.3389/fmars.2019.00436

Derkani, M. H., Alberello, A., Nelli, F., Bennetts, L. G., Hessner, K. G., MacHutchon, K., Reichert, K., Aouf, L., Khan, S., & Toffoli, A. (2021) Wind, waves, and surface currents in the Southern Ocean: observations from the Antarctic Circumnavigation Expedition. *Earth System Science Data, 13*(3), 1189–1209. https://doi.org/10.5194/essd-13-1189-2021

Fedele, F., Lugni, C. & Chawla, A. (2017). The sinking of the El Faro: Predicting real world rogue waves during Hurricane Joaquin. *Scientific Reports, 7*, 11188. https://doi.org/10.1038/s41598-017-11505-5

Garcia, E., Quiles, E. , Correcher, A., & Morant, F. (2018). Sensor buoy system for monitoring renewable marine energy resources. *Sensors, 18*(4), 945. https://doi.org/10.3390/s18040945

Gramcianinov, C. B., Campos, R. M., de Camargo, R., & Guedes Soares, C. (2021). Relation between cyclone evolution and fetch associated with extreme wave events in the South Atlantic Ocean. *Journal of Offshore Mechanics and Arctic Engineering, 143*(6), 1–27. https://doi.org/10.1115/1.4051038

Greig, E., Green, B. A., Ford, H. R., Bertrand Farmer, D., Nottage, K. M., Espinel, Z., & Shultz, K. M. (2020). Extreme population exposure: Hurricane Dorian medical response in Great Abaco, Bahamas. *EClinicalMedicine, 20*, 1002274. https://doi.org/10.1016/j.eclinm.2020.100274

Guillou, N., Lavidas, G., & Chapalain, G. (2020). Wave energy resource assessment for exploitation: A review. *Journal of Marine Science and Engineering, 8*, 705. https://doi.org/10.3390/jmse8090705

Hanson, J. L., & Jensen, R. E. (2004, November). Wave system diagnostics for numerical wave models. *8th International Workshop on Wave Hindcasting and Forecasting, Oahu, Hawaii.* http://www.waveworkshop.org/8thWaves/Papers/E3.pdf

Hanson, J. L., Tracy, B. A., Tolman, H. L., & Scott, R. D. (2009). Pacific hindcast performance of three numerical wave models. *Journal of Atmospheric and Oceanic Technology, 26*(8), 1614-1633. https://doi.org/10.1175/2009jtecho650.1

Hwang, P., & Walsh, E. J. (2018). Propagation directions of ocean surface waves inside tropical cyclones. *Journal of Physical Oceanography, 48*(7), 1495–1511. https://doi.org/10.1175/JPO-D-18-0015.1

Liu, G., Cui, K., Jiang, S., Kou, Y., You, Z., & Yu., P. (2021). A new empirical distribution for the design of wave heights under the impact of typhoons. *Applied Ocean Research, 111*, 102679. https://doi.org/10.1016/j.apor.2021.102679

Longuet-Higgins, M. S., Cartwright, D. E., & Smith, N. D. (1963). Observations of the directional spectrum of sea waves using the motions of a floating buoy. In L. Scriven (Ed.), *Ocean Wave Spectra* (pp. 111–136), Prentice-Hall.

Markina, M. Y., Studholme, J. H. P., & Gulev, S. K. (2019). Ocean wind wave climate responses to wintertime North Atlantic atmospheric transient eddies and low-frequency flow. *Journal of Climate, 32*(17), 5619–5638. https://doi.org/10.1175/JCLI-D-18-0595.1

Meucci, A., Young, I. R., Hemer, M., Kirezci, E., & Ranasinghe, R. (2020). Projected 21st century changes in extreme wind-wave events. *Science Advances, 6*(24), eaaz7295. https://doi.org/10.1126/sciadv.aaz7295

Montoya, R. D., Menendez, M., & Osorio, A. F. (2018). Exploring changes in Caribbean hurricane-induced wave heights. *Ocean Engineering, 163*, 126–135. https://doi.org/10.1016/j.oceaneng.2018.05.032

Nair, M. A., Kumar, V. S., & George, V. (2021). Evolution of wave spectra during sea breeze and tropical cyclone. *Ocean Engineering, 219*, 108341. https://doi.org/10.1016/j.oceaneng.2020.108341

Ortiz-Royero, J. C., Otero, L. J., Restrepo, J. C., Ruiz, J., & Cadena, M. (2013). Cold fronts in the Colombian Caribbean Sea and their 0relationships to extreme wave events. *Natural Hazards Earth System Sciences, 13*, 2797–2804. www.nat-hazards-earth-syst-sci.net/13/2797/2013/

Otero, L. J., Ortiz-Royero, J. C., Ruiz-Merchan, J.K., Higgins, A. E., & Henriquez, S. A. (2016). Storms or cold fronts: What is really responsible for the extreme wave regime in the Colombian Caribbean coastal region? *Natural Hazards Earth System Sciences, 16*, 391–401. https://doi.org/10.5194/nhess-16-391-2016

Ponce de León, S., & Bettencourt, J. H. (2019). Composite analysis of North Atlantic extra-tropical cyclone waves from satellite altimetry observations. *Advances in Space Research*. https://doi.org/10.1016/j.asr.2019.07.021

Pramudya, F. S., Pan, J., Devlin, A. T., & Lin, H. (2021). Enhanced estimation of significant wave height with dual-polarization sentinel-1 SAR imagery. *Remote Sensing, 13*, 124. https://doi.org/10.3390/rs13010124

Ranji, Z., Soltanpour, M., & Shibayama, T. (2020). Spectral analysis of storm-induced waves by Cyclone Ashobaa in Arabian Sea and Gulf of Oman. *Coastal Engineering, 36*(6). https://doi.org/10.9753/icce.v36v.papers.6

Ribal, A., & Young, I. R. (2020). Global calibration and error estimation of altimeter, scatterometer and radiometer wind speed using triple collocation. *Remote Sensing, 12*(12), 1997. https://doi.org/10.3390/rs12121997

Sahoo, B., Jose, F., & Bhaskaran, P. K. (2019). Hydrodynamic response of Bahamas archipelago to storm surge and hurricane generated waves – A case study for Hurricane Joaquin. *Ocean Engineering, 184*, 227–238. https://doi.org/10.1016/j.oceaneng.2019.05.026

Scandurra, G., Romano, A., Ronghi, M., & Carfora, A. (2018). On the vulnerability of Small Island Developing States: a dynamic analysis. *Ecological Indicators, 84*, 382–392. https://doi.org/10.1016/j.ecolind.2017.09.016

Shimura, T., Mori, N., & Hemer, M. A. (2016). Projection of tropical-cyclone generated extreme wave climate based on CMIP5 multi-model ensemble in the Western North Pacific. *Climate Dynamics, 49*, 1449–1462. https://doi.org/10.1007/s00382-016-3390-2

Støle-Hentschel, S., Trulsen, K., Nieto Borge, J.C., & Olluri, S. (2020). Extreme wave statistics in combined and partitioned windsea and swell. *Water Waves, 2*, 169–184. https://doi.org/10.1007/s42286-020-00026-w

Takbash, A., & Young, I. R. (2019). Global ocean extreme wave heights from spatial ensemble data. *Journal of Climate, 32*(20), 6823–6836. https://doi.org/10.1175/JCLI-D-19-0255.1

Tamizi, A., & Young, I. R. (2020). The spatial distribution of ocean waves in tropical cyclones. *Journal of Physical Oceanography, 50*(8), 2123–2139. https://doi.org/10.1175/JPO-D-20-0020.1

Thomas, A., Baptiste, A., Martyr-Koller, R. Pringle, P., & Rhiney, K. (2020). Climate change and Small Island Developing States. *Annual Review of Environment and Resources, 45*(1), 1–27. https://doi.org/10.1146/annurev-environ-012320-083355

Tian, D., Zhang, H., Zhang, W., Zhou, F., Sun, X., Zhou, Y., & Ke, D. (2020). Wave glider observations of surface waves during three tropical cyclones in the South China Sea. *Water, 12*(5), 1331. https://doi.org/10.3390/w12051331

Timmermans, B., Patricola, C., & Wehner, M. (2018). Simulation and analysis of hurricane-driven extreme wave climate under two ocean warming scenarios. *Oceanography, 31*(2), 88–99. https://doi.org/10.5670/oceanog.2018.218

Wang, J., Aouf, L., Wang, X., Li, B., & Wang, J. (2020). Remote cross-calibration of wave buoys based on significant wave height observations of altimeters in the Northern Hemisphere. *Remote Sensing, 12*, 3447. https://doi.org/10.3390/rs12203447

Yang, S., & Oh, J. (2018). Long-term changes in the extreme significant wave heights on the Western North Pacific: Impacts of tropical cyclone activity and ENSO. *Journal of Atmospheric Science, 54*(1), 103–103. https://doi.org/10.1007/s13143-017-0063-y

Zegarra, M. A., Schmid, J. P., Palomino, L. & Seminario, B. (2020). *Impact of Hurricane Dorian in The Bahamas: A view from the sky.* InterAmerican Development Bank. https://doi.org/10.18235/0002163

Zhang, B., Li, X., Perrie, W., & He, Y. (2015). Synergistic measurements of ocean winds and waves from SAR. *Journal of Geophysical Research: Oceans, 120*, 6164–6184. https://doi.org/10.1002/2015JC011052